INFECTION AND IMMUNITY, May 2008, p. 2002–2007
0019-9567/08/$08.00+0 doi:10.1128/IAI.01588-07

Vol. 76, No. 5

Mycolactone Is Responsible for the Painlessness of *Mycobacterium ulcerans* Infection (Buruli Ulcer) in a Murine Study▽

Junichiro En,[1,2] Masamichi Goto,[1]* Kazue Nakanaga,[3] Michiyo Higashi,[1] Norihisa Ishii,[3] Hajime Saito,[4] Suguru Yonezawa,[1] Hirofumi Hamada,[5] and Pamela L. C. Small[6]

Department of Human Pathology, Kagoshima University Graduate School of Medical and Dental Sciences, Kagoshima, Japan[1]; National Sanatorium Hoshizuka-Keiaien, Kagoshima, Japan[2]; Leprosy Research Center, National Institute of Infectious Diseases, Tokyo, Japan[3]; Hiroshima Environment and Health Association, Hiroshima, Japan[4]; Kagoshima University Graduate School of Health Sciences, Kagoshima, Japan[5]; and Department of Microbiology, University of Tennessee, Knoxville, Tennessee 37996-0845[6]

Received 2 December 2007 Returned for modification 10 January 2008/Accepted 19 February 2008

Buruli ulcer is a chronic skin disease caused by *Mycobacterium ulcerans*, which produces a toxic lipid mycolactone. Despite the extensive necrosis and tissue damage, the lesions are painless. This absence of pain prevents patients from seeking early treatment and, as a result, many patients experience severe sequelae, including limb amputation. We have reported that mice inoculated with *M. ulcerans* show loss of pain sensation and nerve degeneration. However, the molecules responsible for the nerve damage have not been identified. In order to clarify whether mycolactone alone can induce nerve damage, mycolactone A/B was injected to footpads of BALB/c mice. A total of 100 μg of mycolactone induced footpad swelling, redness, and erosion. The von Frey sensory test showed hyperesthesia on day 7, recovery on day 21, and hypoesthesia on day 28. Histologically, the footpads showed epidermal erosion, moderate stromal edema, and moderate neutrophilic infiltration up to day 14, which gradually resolved. Nerve bundles showed intraneural hemorrhage, neutrophilic infiltration, and loss of Schwann cell nuclei on days 7 and 14. Ultrastructurally, vacuolar change of myelin started on day 14 and gradually subsided by day 42, but the density of myelinated fibers remained low. This study demonstrated that initial hyperesthesia is followed by sensory recovery and final hypoesthesia. Our present study suggests that mycolactone directly damages nerves and is responsible for the absence of pain characteristic of Buruli ulcer. Furthermore, mice injected with 200 μg of mycolactone showed pulmonary hemorrhage. This is the first study to demonstrate the systemic effects of mycolactone.

Buruli ulcer is a chronic painless skin disease caused *by Mycobacterium ulcerans* (12, 14). *M. ulcerans* produces a toxic lipid, mycolactone, that induces apoptosis in guinea pig lesions, as well as in human patients (6, 13). Painlessness is a major characteristic of Buruli ulcer, and this phenomenon may often lead the patients to underestimate the disease, which can interfere with the early diagnosis and effective treatment, resulting in severe sequelae such as limb amputation. However, the mechanism of the painlessness was obscure. We have recently reported that in mice inoculated with *M. ulcerans*, nerve bundles are invaded and damaged by the bacilli (8). Whether the nerve damage was due to mechanical compression by the invaded bacilli or due to the chemical substance(s) produced by the bacilli remained unclear.

In this study, we examined whether mycolactone alone can induce lesions in mice footpads similar to those produced by *M. ulcerans* inoculation. Sensory changes, footpad swelling, and detailed histopathology, including the ultrastructure of the peripheral nerves, were studied. By comparing the kinetics of pain loss, we tried to reveal the characteristics of neurotoxicity of mycolactone.

* Corresponding author. Mailing address: Department of Human Pathology, Kagoshima University Graduate School of Medical and Dental Sciences, 8-35-1 Sakuragaoka, Kagoshima 890-8544, Japan. Phone: 81-99-275-5270. Fax: 81-99-265-7235. E-mail: masagoto@m2.kufm.kagoshima-u.ac.jp.

▽ Published ahead of print on 3 March 2008.

MATERIALS AND METHODS

Mycolactone injection. The animal experiment was approved by Kagoshima University Committee of Animal Experiments. Initial experiments were conducted to determine the optimal concentrations of mycolactone for studies of pain loss. Mycolactone A/B was isolated from *M. ulcerans* 1615 and purified initially using a 2:1 chloroform extract. Lipids in this extract were subsequently separated by a centrifugal thin-layer chromatograph (Chromatotron; Harrison Research, Palo Alto, CA). The purity of mycolactone preparation was confirmed by mass spectroscopy (6). One mg of mycolactone A/B isolated from *M. ulcerans* 1615 was dissolved in 25 μl of ethanol and further diluted by 7H9 broth. Mycolactone at 1, 3, 10, 30, 100, or 200 μg in 25 μl of final volume was used as the inoculum. 7H9 broth (25 μl) containing 5 μl of ethanol served as a control. Each solution was injected into the left footpad of 35 6-week-old female BALB/c mice (1 μg, $n = 4$; 3 μg, $n = 4$; 10 μg, $n = 3$; 30 μg, $n = 5$; 100 μg, $n = 5$; 200 μg, $n = 5$; control, $n = 9$). Morphological studies were done on day 7.

In the second series of experiment, 100 μg of mycolactone was injected into the left footpad of 30 6-week-old female BALB/c mice (100 μg, $n = 25$; control, $n = 5$). Sensory and morphological studies were done on days 7 to 42.

Sensory test and thickness of footpads. In order to examine whether the lesions are painless or not, a behavioral test was performed (8). Briefly, mechanical force to the dorsum of the mouse footpads from the bottom of punched metal floor was measured by using von Frey monofilaments (Touch-Test Sensory Evaluator Instrument; North Coast Medical, Inc., Morgan Hill, CA). Each animal was stimulated three times with filaments using pressures of 0.02, 0.04, 0.07, 0.4, 1, 4, or 10 g. If the animal raised the stimulated foot, it was counted as positive response. The data of animals were summed up in each group. After each sensory test, the thickness of the foot was measured with a caliper.

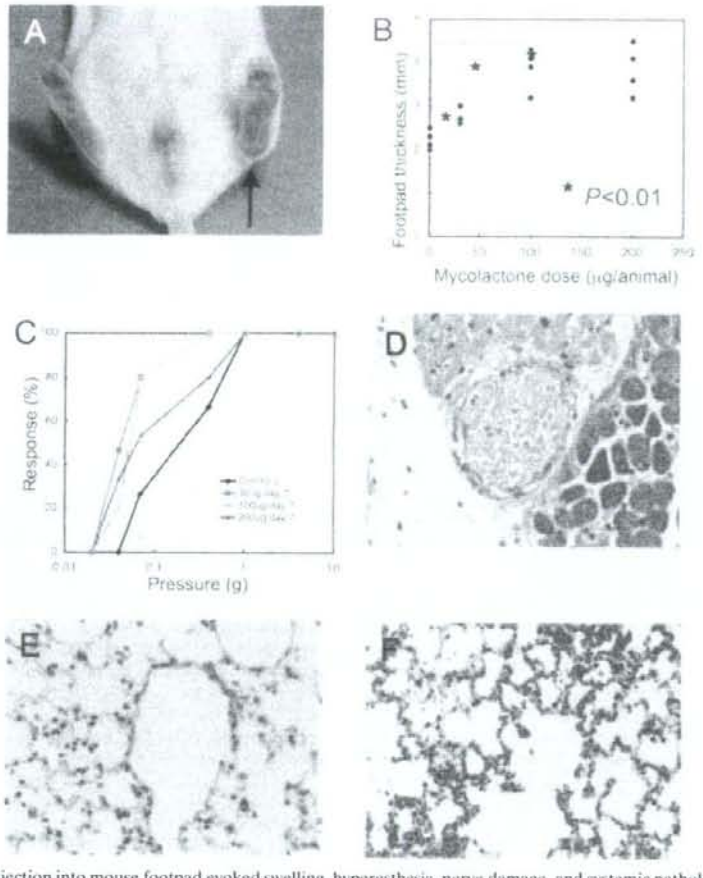

FIG. 1. Mycolactone injection into mouse footpad evoked swelling, hyperesthesia, nerve damage and systemic pathology. Various amounts (30, 100, and 200 μg) of mycolactone A/B were injected into the left footpads of BALB/c mice. (A) Footpad swelling on day 7 after the injection of 100 μg (arrow). (B) Footpad thickness on day 7. Dose-dependent swelling was significant. (C) Sensory test showing hyperesthesia on day 7 ($P = 0.02$). (D) Nerve bundles showed a loss of Schwann cell nuclei and intraneural hemorrhage (H&E; magnification, ×168). (E) Lung without mycolactone injection (H&E, magnification, ×168). (F) Intra-alveolar hemorrhage in the lungs of mice injected with 200 μg of mycolactone into the footpad (H&E, magnification, ×168).

Histology and electron microscopy of footpads. In the initial study, 35 animals in total (1 μg, $n = 4$; 3 μg, $n = 4$; 10 μg, $n = 3$; 30 μg, $n = 5$; 100 μg, $n = 5$; 200 μg, $n = 5$; control, $n = 9$) were examined. After induction of deep anesthesia, perfusion fixation was performed with 4% paraformaldehyde and 0.1% glutaradehyde in phosphate buffer (1 μg, $n = 4$; 3 μg, $n = 4$; 10 μg, $n = 3$; 30 μg, $n = 3$; 100 μg, $n = 3$; 200 μg, $n = 3$; control, $n = 7$) and with 4% paraformaldehyde and 1% glutaradehyde in phosphate buffer (30 μg, $n = 2$; 100 μg, $n = 2$; 200 μg, $n = 2$; control, $n = 2$). For the histological study, hind limbs and general organs were embedded in paraffin, cut into 4-μm sections, and examined by hematoxylin and eosin (H&E;) staining. For the electron microscopic study, hind limbs were postfixed with osmium tetroxide and embedded into Epon. Toluidine blue-stained 1-μm sections were screened, and nerve bundles were ultrathin sectioned and stained with uranium and lead for electron microscopy.

A TUNEL (terminal deoxynucleotidyltransferase-mediated dUTP-biotin nick end labeling) assay was performed by using an Apoptag kit (S7110; Chemicon International, Inc., Temecula, CA). Paraffin sections were treated with 20 μg of proteinase K/ml and then with 3% hydrogen peroxide in phosphate-buffered saline (PBS) before being washed with distilled water. Equilibration buffer was added and the mixture was incubated with terminal deoxynucleotidyltransferase for 1 h at 37°C. Stop/wash buffer was then applied for 10 min. After a wash with PBS, anti-digoxigenin conjugate was added, and the mixture was incubated at room temperature for 30 min. After a wash with PBS and color development with a peroxidase substrate, the specimens were counterstained with methyl green.

In the second series of experiment, 30 animals in total (100 μg, $n = 25$; control, $n = 5$) were examined. Perfusion fixation was performed with 4% paraformaldehyde and 0.1% glutaradehyde for the histological study (100 μg on days 7, 14, 21, 28, and 42, $n = 3$ each; control on day 42, $n = 3$) and with 4% paraformaldehyde and 1% glutaradehyde for the electron microscopic study (100 μg on days 7, 14, 21, 28, and 42, $n = 2$ each; control on day 42, $n = 2$). Histological and electron microscopic procedures were performed in the same manner.

RESULTS

In the initial experiment, 1, 3, or 10 μg of mycolactone did not induce significant gross or histological changes. Significant changes were also not observed in Epon sections. However, 30, 100, or 200 μg of mycolactone induced local swelling (footpad thickness on day 7, control, 2.2 mm; 30 μg, 2.8 mm; 100 μg, 3.7

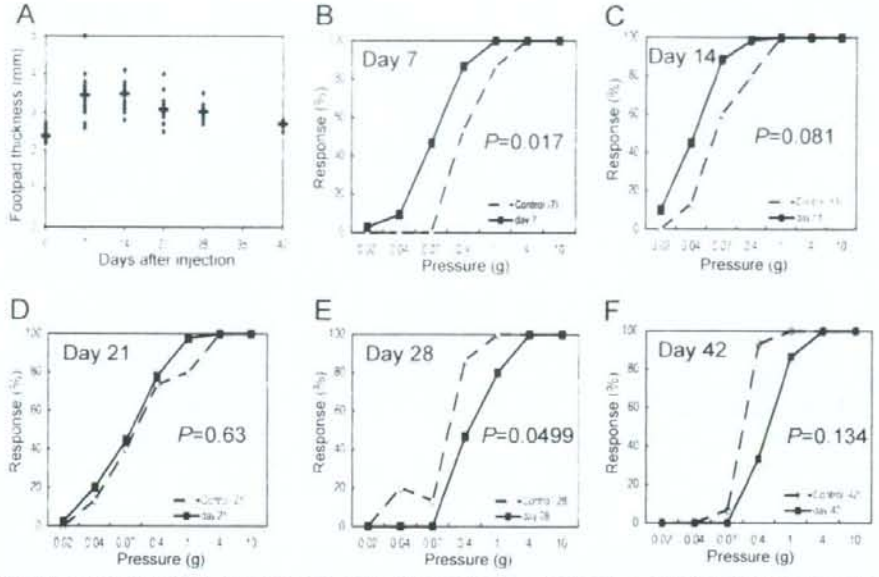

FIG. 2. Sequential analysis of footpad thickness and sensation after mycolactone injection (100 μg). (A) Footpad thickness after mycolactone injection showed the peak swelling on day 14, with subsequent resolution. Sensory test showed significant hyperesthesia on day 7 (B, $P = 0.017$) and hyperesthetic tendency on day 14 (C, $P = 0.081$), normal sense on day 21 (D, $P = 0.63$), followed by significant hypoesthesia on day 28 (E, $P = 0.0499$) and hypoesthetic tendency on day 42 (F, $P = 0.13$).

mm; 200 μg, 3.7 mm) ($P < 0.01$ between control and each dose), redness, and erosion at the injected site (Fig. 1A and B). A sensory test showed no significant changes on day 4, but hyperesthesia was noted on day 7 (Fig. 1C) ($P = 0.022$ between the control and the 30-μg injection, $P = 0.024$ between the control and all of the other injections).

Histological examination of the footpads on day 7 after the injection of 30, 100, and 200 μg of mycolactone revealed focal epidermal erosion, moderate stromal edema, mild fibrinous exudates, and mild infiltration of neutrophils. Blood vessels showed high endothelial venule, and focal hemorrhage was observed. Nerve bundles showed a loss of Schwann cell nuclei (Fig. 1D) and/or intraneural hemorrhage beneath the erosion. Some Schwann cells showed nonspecific degeneration, but intracytoplasmic vacuoles observed in *M. ulcerans* inoculation was not yet identified. Nerve damage and the number of infiltrating neutrophils showed no significant differences between the low-dose mycolactone (30 μg) and high-dose mycolactone (100 and 200 μg) samples. However, the extent of fibrinous exudate and stromal edema was more prominent in high-dose injections than in low-dose injections. In the control animals, no histological change was observed.

Apoptosis was demonstrated by using the TUNEL method in some Schwann cells after injection of mycolactone (30 and 200 μg). However, similar apoptosis was observed in the Schwann cells of control animals, and there was no significant difference between the mice with mycolactone injection and those of negative controls.

After the injection of 200 μg of mycolactone into the footpad, significant nerve damage was observed in the back of the foot, but 30- and 100-μg injections produced no nerve damage in this region. Inflammation and edema in the back of foot was absent in the 30-μg injection animals, mild in the 100-μg injection animals, and marked in the 200 μg-injection animals. An ulcer was not observed in the back of foot at any of the doses used.

Systemic effects of mycolactone were also observed at the highest concentration. Injection of 200 μg of mycolactone into the foot produced multiple hemorrhages in the lungs (control, Fig. 1E; 200 μg of mycolactone, Fig. 1F), whereas injection of 100 or 200 μg yielded mild swelling in the spleen. No significant changes were observed in the thymus, liver, and small intestine after mycolactone injection.

In the second experiment, we tried to evaluate chronological changes produced by mycolactone injection by using a sensory test and morphology in order to determine whether hyperesthesia observed in the first experiment is a transient phenomenon followed by hypoesthesia and whether mycolactone is sufficient to induce vacuolar changes of Schwann cell cytoplasm. Thickness after mycolactone injection (100 μg) showed peak swelling on day 14, with subsequent resolution (Fig. 2A). A sensory test showed significant hyperesthesia on day 7 (Fig. 2B, $P = 0.017$) and hyperesthetic tendency on day 14 (Fig. 2C, $P = 0.081$), normal sense on day 21 (Fig. 2D, $P = 0.63$), followed by significant hypoesthesia on day 28 (Fig. 2E, $P = 0.0499$) and hypoesthetic tendency on day 42 (Fig. 2F, $P = 0.134$).

Nerves in the footpads of control mice (only ethanol and 7H9 broth injected, Epon section) showed no significant change (Fig. 3A). In the longitudinal morphological study of

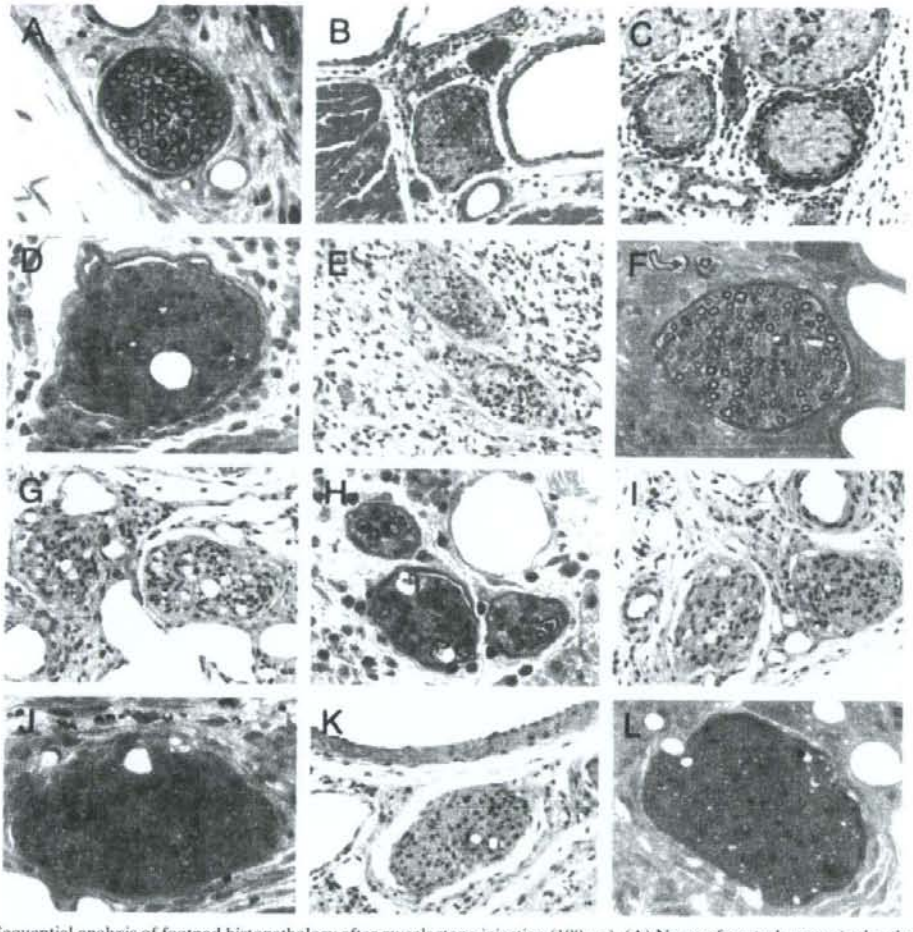

FIG. 3. Sequential analysis of footpad histopathology after mycolactone injection (100 μg). (A) Nerve of control mouse (only ethanol and 7H9 broth injected) showed no significant change. (B to D) On day 7, nerves of mycolactone-injected mice showed intraneural hemorrhage (B) and massive neutrophilic infiltration to the perineurium (C). (D) Epon section showing moderate loss of nerve fibers and myelin. (E and F) Nerves on day 14 showed intraneural inflammatory cell infiltration and hemorrhage. (G) Nerves on day 21. Mild infiltration inflammatory cell infiltration and vacuolar change were observed. (H) Vacuolar change of Schwann cells induced by mycolactone injection on day 21 was similar to *M. ulcerans* inoculation. (I) In the nerves on day 28, histological damage remained. (J) Thin myelins indicating remyelination were observed on day 28. (K) In the nerves on day 42, when sensory disturbance lasted, histological damage remained. (L) Mild fibrosis was observed on day 42. (A, D, F, H, J, and L [Epon, 1-μm sections, toluidine blue staining], magnification, ×340; B, C, E, G, I, and K [paraffin sections, H&E staining], magnification, ×157).

mycolactone-injected nerves, the nerves in the footpads of mycolactone-injected mice on day 7 showed intraneural hemorrhage (Fig. 3B) and massive neutrophilic infiltration to perineurium (Fig. 3C). Vacuolar changes of Schwann cells were not observed. Epon sections showed moderate loss of nerve fibers and myelin (Fig. 3D). Intraneural inflammatory cell infiltration and hemorrhage (Fig. 3E and F) were observed in nerves on day 14. On day 21, when the sensory test recovered to normal, nerves exhibited mild inflammatory cell infiltration and vacuolar changes (Fig. 3G). Vacuolar changes observed in Schwann cells induced by mycolactone injection on day 21 was similar to that found previously with *M. ulcerans* inoculation (Fig. 3H). On day 28, when sensory disturbance was detected by von Frey sensory test, histological damage remained was still evident in nerves (Fig. 3I). Thin myelin indicating remyelination was observed on day 28 (Fig. 3J). Nerves on day 42, when sensory disturbance lasted, histological damage remained (Fig. 3K). Mild fibrosis was observed on day 42 (Fig. 3L).

Electron micrographs showed intraneural infiltration of lymphocyte and macrophage containing myelin debris on day 14 after mycolactone injection (Fig. 4A). On day 21, perineural infiltration of neutrophil, vacuolar change of myelin, and macrophage were observed (Fig. 4B). On day 28, thin myelins

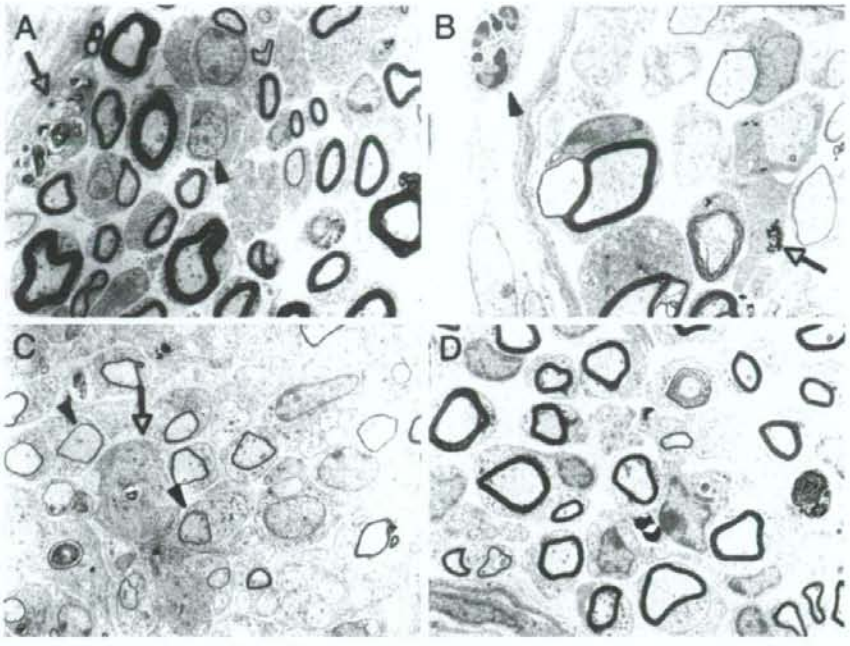

FIG. 4. Ultrastructure of nerves after mycolactone injection. (A) Intraneural infiltration of lymphocytes (arrowhead) and macrophage (arrow) containing myelin debris on day 14 after mycolactone injection. (B) Vacuolar change of myelin (*) and macrophage (arrow) on day 21. (C) Thin myelins (arrows) indicate remyelination on day 28. D. Mild fibrosis observed on day 42. (Epon-embedded ultrathin sections stained by uranium and lead; magnification, ×1,960).

indicating remyelination and infiltration of macrophage (arrow) were detected (Fig. 4C). On day 42, myelins of normal thickness were observed, a finding which indicates the completion of remyelination (Fig. 4D).

DISCUSSION

The lack of pain in Buruli ulcer has been one of the most puzzling and remarkable characteristics of this condition. However, until recently, the pathogenesis of painlessness in Buruli ulcer has not been studied. By a careful study of BALB/c mice inoculated by *M. ulcerans*, Addo et al. observed that mice failed to withdraw their limbs when pricked with a needle at the stage of foot-thigh edema or foot ulceration (1). These results suggested the presence of peripheral anesthesia. We have also demonstrated decreased response to the sensory test of mouse footpads accompanied by moderate swelling and erosion and demonstrated bacterial invasion into the nerves associated with nerve damage by using histopathological and ultrastructural studies (8). In these studies the ability of *M. ulcerans* to evoke nerve damage became clear; however, the exact molecule causing the nerve damage was not identified.

We report here that the *M. ulcerans* toxin, mycolactone, is sufficient to cause neurological damage. By studying the kinetics of sensory response after mycolactone injection, we have shown that the response shifted from hypersensitivity (days 7 and 14) to normal (day 21) to hyposensitivity (days 28 and 42), while morphological changes advanced up to day 42. Hypersensitivity seems to be induced by acute inflammation, as demonstrated by the dense neutrophilic infiltration into the perineurium and intraneural hemorrhage. Oliveira et al. (10) and Coutanceau et al. (4) also demonstrated a persistent neutrophilic infiltrate in *M. ulcerans*-injected mice, which resembles the findings in our mycolactone study. We suggest that the later hyposensitive phase is due to the resolution of the inflammatory reaction, associated with the loss of axons and fibrosis. Another interesting finding in our study is the remyelination observed on day 28. This was not observed after the injection of *M. ulcerans* (8). Among the clinical forms of Buruli ulcer, the edematous lesion is usually painful (3). This may be reflected in our early stage of mycolactone injection. As a negative control, control extract from mycolactone-negative *M. ulcerans* strains was not available. Thus, we used the same amount of mycolactone solvent (ethanol) as that used for mycolactone fluid preparation. This might have somewhat interfered with our results.

By injecting 100 μg of mycolactone into the backs of guinea pigs, George et al. (7) could induce pathological lesions characteristic of Buruli ulcer at the injection sites. These researchers also observed slight erythema near the injection site of 10 μg but no gross pathology caused by 1 μg (6). Since BALB/c mice have smaller bodies than guinea pigs, we initially expected that lesions could be induced by 1, 3, or 10 μg. However, no lesion was evoked by 1, 3, or 10 μg of mycolactone, and thus we had to increase the amount to 30, 100, and 200 μg

in order to produce pathological findings. Injections of 100 and 200 μg induced similar lesions, but 30 μg produced milder lesions. Based on these data, we used 100 μg of mycolactone for the sequential analysis of footpad lesions. Mycolactone can induce fat necrosis (6); however, murine skin contains considerably less fat than is present in human or guinea pig skin. This may partially explain the higher amount of mycolactone required to produce pathology in murine skin.

In this study, we could not demonstrate significant apoptosis by mycolactone injection. Early work demonstrated that mycolactone can cause apoptosis on murine fibroblasts at very low concentrations of 2 pg/ml (6, 7). Dobos et al. suggested that *M. ulcerans* might secrete a proteinenous toxin which caused necrosis (5), but in that study the protein fractions may have been contaminated with mycolactone (2). A recent study reports that concentrations of mycolactone greater than 15 μg/ml causes necrosis of L929 fibroblasts as measured by lactate dehydrogenase release (2).A total of 100 μg of mycolactone in our experiment is thought to be a much higher dose than the minimal dose required for causing apoptosis, and necrosis seems to have been the predominant pathology produced in our experiment.

Our study is the first to show that the nerve damage and painlessness associated with Buruli ulcer can be induced by mycolactone alone. Mycolactone injection induced hyperesthesia in the early stage, followed by sensory loss. Morphologically, various nerve lesions, including neutrophilic infiltration, hemorrhage, necrosis, vacuolation of Schwann cell cytoplasm, remyelination, and fibrosis, were observed. This study demonstrated that reversible nerve damage can be induced by a single injection of mycolactone to mouse footpad and suggests that nerve damage induced by mycolactone is responsible for the abnormal sensation, especially painlessness, associated with Buruli ulcer.

Although Buruli ulcer is usually a focal disease, severe forms of the disease occur, including osteomyelitis and disseminated disease (11). Histopathology was found in lymph nodes adjacent to a lesion, suggesting that mycolactone-induced pathology might occur distant from the site of ulceration (9). The persistence of mycolactone in tissue is unknown, although it is likely that the molecule would be degraded by host esterases. In our study it is clear that mycolactone alone can induce pathology at sites distant from the site of inoculation.

In human lesions microhemorrhage is a characteristic finding. Our results suggest that mycolactone is sufficient to induce microhemorrhage. In summary, the present study shows for the first time that mycolactone produces nerve damage leading to painlessness and can also act at sites distant from the site of inoculation. To better understand mycolactone-mediated pathology further studies are needed to determine the kinetics of mycolactone in vivo as well as to determine how the molecule may be transported to distant tissues.

Editor: F. C. Fang

ACKNOWLEDGMENTS

This research was supported by grants from the U.S.-Japan Cooperative Medical Science Program, Ministry of Health, Labor, and Welfare (2007-IM [assigned]-002), and the International Medical Centre, Japan (International Cooperation Research Grant, topic code 18C4).

We are grateful to T. Hatanaka, K. Sakazume, Y. Nishimura, and Y. Arimura for technical assistance.

REFERENCES

1. **Addo, P., E. Owusu, B. Adu-Addai, M. Quartey, M. Abbas, A. Doddo, and D. Ofori-Adjei.** 2005. Findings from a Buruli ulcer mouse model study. Ghana Med. J. **39:**86–93.
2. **Adusumilli, S., A. Mve-Obiang, T. Sparer, W. Meyers, J. Hayman, and P. L. Small.** 2005. *Mycobacterium ulcerans* toxic macrolide, mycolactone modulates the host immune response and cellular location of *M. ulcerans* in vitro and in vivo. Cell Microbiol. **7:**1295–1304.
3. **Asiedu, K., W. Meyers, and P. Agbenorku.** 2000. Clinical features and treatment, p. 37–38. *In* K. Asiedu, R. Scherpbier, and M. Raviglione (ed.), Buruli ulcer *Mycobacterium ulcerans* infection. World Health Organization, Geneva, Switzerland.
4. **Coutanceau, E., P. Legras, L. Marsollier, G. Reysset, S. T. Cole, and C. Demangel.** 2006. Immunogenicity of *Mycobacterium ulcerans* Hsp65 and protective efficacy of a *Mycobacterium leprae* Hsp65-based DNA vaccine against Buruli ulcer. Microbes Infect. **8:**2075–2081.
5. **Dobos, K. M., P. L. Small, M. Deslauriers, F. D. Quinn, and C. H. King.** 2001. *Mycobacterium ulcerans* cytotoxicity in an adipose cell model. Infect. Immun. **69:**7182–7186.
6. **George, K. M., D. Chatterjee, G. Gunawardana, D. Welty, J. Hayman, R. Lee, and P. L. Small.** 1999. Mycolactone: a polyketide toxin from *Mycobacterium ulcerans* required for virulence. Science **283:**854–857.
7. **George, K. M., L. Pascopella, D. M. Welty, and P. L. Small.** 2000. A *Mycobacterium ulcerans* toxin, mycolactone, causes apoptosis in guinea pig ulcers and tissue culture cells. Infect. Immun. **68:**877–883.
8. **Goto, M., K. Nakanaga, T. Aung, T. Hamada, N. Yamada, M. Nomoto, S. Kitajima, N. Ishii, S. Yonezawa, and H. Saito.** 2006. Nerve damage in *Mycobacterium ulcerans*-infected mice: probable cause of painlessness in Buruli ulcer. Am. J. Pathol. **168:**805–811.
9. **Meyers, W. M.** 2001. Histopathological methods, p. 37–46. *In* F. Portaels, P. Johnson, and W. M. Meyers (ed.), Diagnosis of *Mycobacterium ulcerans* disease (Buruli ulcer), World Health Organization, Geneva, Switzerland.
10. **Oliveira, M. S., A. G. Fraga, E. Torrado, A. G. Castro, J. P. Pereira, A. L. Filho, F. Milanezi, F. C. Schmitt, W. M. Meyers, F. Portaels, M. T. Silva, and J. Pedrosa.** 2005. Infection with *Mycobacterium ulcerans* induces persistent inflammatory responses in mice. Infect. Immun. **73:**6299–6310.
11. **Pszolla, N., M. R. Sarkar, W. Strecker, P. Kern, L. Kinzl, W. M. Meyers, and F. Portaels.** 2003. Buruli ulcer: a systemic disease. Clin. Infect. Dis. **37:**e78–e82.
12. **Sizaire, V., F. Nackers, E. Comte, and F. Portaels.** 2006. *Mycobacterium ulcerans* infection: control, diagnosis, and treatment. Lancet Infect. Dis. **6:**288–296.
13. **Walsh, D. S., W. M. Meyers, F. Portaels, J. E. Lane, D. Mongkolsirichaikul, K. Hussem, P. Gosi, and K. S. Myint.** 2005. High rates of apoptosis in human *Mycobacterium ulcerans* culture-positive Buruli ulcer skin lesions. Am. J. Trop. Med. Hyg. **73:**410–415.
14. **Wansbrough-Jones, M., and R. Phillips.** 2006. Buruli ulcer: emerging from obscurity. Lancet **367:**1849–1858.

13 結 核 菌

【病原体の特性，BSL】（表1）

結核は古代から人類を脅かしてきた感染症であるが，未だ制圧されていない．結核菌既感染者は全世界で約20億人（日本：2,500万人），年間新規患者数は880万人（日本：2.6万人），罹患率（対人口10万人）は140（日本：20.6），年間死亡者数は200万人（日本：0.23万人）であり，現在においても甚大な健康被害を提供している．病変部位により，肺結核，肺外結核，粟粒（全身播種性）結核に分類される．

結核菌は *Mycobacterium* 属（抗酸菌）に属し，非運動性，芽胞や莢膜を形成しない好気性グラム陽性桿菌（長さ：2～4 μm，幅：0.3～0.6 μm）である．ゲノムサイズは約4.4 Mbでgc比65.6％である．遺伝学的にきわめて近縁の *M. bovis*, *M. africanum* や *M. microti* とともに結核菌群 *Mycobacterium tuberculosis* complex を形成している．結核菌群は生化学的にナイアシンを産生することで，非結核性抗酸菌やらい菌等の他の抗酸菌と区別される．抗酸菌細胞壁は脂質に富むため（乾燥菌量の10～40％，細胞壁の20～60％），通常のグラム染色法では染色されにくく，Ziehl-Neelsen法や蛍光等の特殊染色（抗酸性染色）によって染色される．しかし，いったん染色されると塩酸等でも脱色されにくいことから抗酸菌（acid-fast bacilli）と呼ぶ．細胞壁糖脂質，特に，ミコール酸（mycolic acid）は染色性や細胞壁の疎水性に最も関与している．菌体表層の強い疎水性のため，乾燥，凍結や酸・アルカリ，消毒剤等に強い抵抗性を示し，宿主体内外で長期間にわたり生存する．

発育には適度の酸素（20％）を必要とし，炭酸ガス（5％）は発育を促進させる．しかし，嫌気状態でも完全に死滅することはなく，休眠状態（dormancy）として生存する．37～38℃を発育至適温度とし，至適pHはpH6.8～7.0である．固形培地として，小川培地やLowenstein-Jensen培地等の卵培地，あるいは，Middlebrook 7H10や7H11培地が使用されるが，遅発育性であり（倍加時間：16～18時間），コロニーの肉眼的な検出に2～3週間以上を要する．遅発育性は検体培養による結核の診断を遅らせる一因となる．小川培地表面では「ロウ状」の光沢を持ったR型コロニーを形成し，乳白色～淡黄色の色調を呈する．界面活性剤を加えずに液体培地に培養した場合，培地表面に肉眼的にコード状に発育する（cord形成）．

喀痰に含まれる結核菌の飛沫核（空気）感染により，結核はヒト-ヒト感染伝播する．結核菌は病原性の高い細菌であり，わずか数個の菌を吸入することで感染が成立する．感染しても発病は生涯を通じて約10％で，90％は感染した結核菌が休眠状態で宿主体内に残存する（persister）．

結核菌は外毒素や内毒素を産生せず，その病原性は宿主感染防御機構から逸脱して細胞内生存や増殖をすること，遅延型過敏反応を誘導することにより表現される．結核菌は細胞内寄生菌であり，宿主マクロファージに貪食された後，殺菌されずに増殖する．マクロファージ内では食胞体（ファゴゾーム）内に留まるが，ファゴゾームとリソゾームの融合（ファゴリソゾーム融合）を阻害することで，細胞内殺菌機構から逸脱する．

すべての結核菌株はBSL-3である．

感染症の予防及び感染症の患者に対する医療に関する法律等の一部を改正する法律（改正感染症法）では，結核菌は特定病原体等に指定され，四種病原体等に，多剤耐性結核菌は三種病原体等に分類されるので，管理・取扱いに際し，同法を遵

表1　結核菌の特徴

細胞内寄生性	ファゴリソゾーム融合を阻害し，マクロファージ内ファゴソーム中で生存
遅発育性	倍加時間 16～18 時間 コロニー形成に 2～3 週間以上
細胞壁	脂質に富み（乾燥菌量の 10～40%，細胞壁の 20～60%），抗酸性を呈する 種々の環境や化学物質に抵抗性を示す
運動性	非運動性，芽胞非形成性，莢膜なし
遺伝子	ゲノムサイズ約 4.4 Mb，GC 比 65.6%
感染形式	エアロゾル：飛沫核（空気）感染
好気性	発育には酸素を要求し，酸素分圧の高い肺等で増殖 酸素が枯渇しても死滅せず，休眠状態となる
病態	慢性炎症，肉芽腫形成，乾酪壊死，空洞形成，線維化

表2　結核菌曝露に対する応急措置，及び事故対応

バイオセーフティレベル		BSL-3
感染経路		結核菌を含む飛沫核（空気）感染
応急処置	針刺し・怪我	血液を絞り出し，流水で洗浄後，傷口を消毒
	皮膚	流水で洗浄後，消毒
	口	うがい
	眼	流水あるいは滅菌生理食塩水で洗浄
	鼻	鼻腔洗浄
感染事故対応		応急処置と施設管理者への報告，医療機関を受診
緊急投薬		なし
有効な薬剤		発病予防にはイソニアジド（INH）投与，INH 耐性菌の場合，リファンピシン（RIF）投与
経過観察		定期健診による胸部 X 線撮影検査 結核菌特異抗原による末梢血 interferon-γ 遊離試験 ツベルクリン皮内反応検査 経過観察，曝露後 2 年間
臨床症状		針刺し・外傷局所では感染部位の炎症，所属リンパ節の腫脹 症状は 2 週間以上持続する咳嗽，喀痰や発熱が最も多く，その他，全身倦怠，血痰，胸痛，体重減少，寝汗や食欲低下等

表3　結核菌感染に対する予防措置

ワクチンの接種		BCG ワクチン
特異免疫反応試験	TST	ツベルクリン皮内反応（Mantoux） 48 時間後判定：遅延型皮内反応
	IGRA：QFT	末梢血細胞 IFN-γ 産生・遊離試験（IGRA，Quantiferon®）：*in vitro* 抗原：ESAT-6，CFP-10
発病予防内服		感染曝露が確認された場合，INH（300 mg/日，6～9 ケ月）投与，INH 耐性菌の場合，リファンピシン（RIF）投与
滅菌法		使用した器具はオートクレーブ 121℃，30 分による滅菌
消毒薬		アルコール類，フェノール類，アルデヒド類による消毒

守する．

【実験室のハザード及び予想されるリスク】(表2)

結核菌は飛沫核（エアロゾル）により感染伝播するので，実験室においてはエアロゾルの発生及び吸引に留意する．1979～1999年における実験室感染の原因病原体の中で，結核菌は最も頻度が高かった．針刺し，外傷等により菌が体内に入った可能性のある場合，緊急処置を必要とする．また，有効な抗微生物薬の投与を行う．針刺しや外傷では感染部位の炎症，所属リンパ節の腫脹が生じる．針刺しや外傷に対しては，血液を絞り出し，流水で洗浄後，創部を消毒する．体表面への付着が懸念される場合には流水で洗浄し，可能であれば消毒する．口腔内に入った可能性がある場合には十分にうがいを行う．感染事故対応は，針刺し事故等の場合には応急処置と施設管理者への報告，医療機関の受診を行う．なお，結核予防法は改正感染症法に統合され，結核は二類感染症に位置づけられた．この規程により，結核患者あるいは結核の疑い患者と診断するに足る高度の蓋然性が認められる場合，診察した医師は届出を直ちに行わなければならない．

臨床症状としては2週間以上持続する咳嗽，喀痰や発熱が最も多い．全身倦怠，血痰，胸痛，体重減少，寝汗や食欲低下等を伴うこともある．なお，約20%は自覚症状の有無に関わらず，健康診断で発見される．

本菌の潜伏期間は長く，若年層の一次感染では4～18ケ月，既感染者の二次感染では長期経過後の発症もある．そのため，感染が懸念される場合，胸部X線撮影検査，感染曝露6～8週間後，結核菌特異抗原による末梢血interferon-γ遊離試験（Quantiferon® 陽性：0.35IU/mL以上）やツベルクリン皮内反応検査（陽性，日本：紅斑≧直径10 mm以上，欧米：硬結≧直径5 mm以上）等を行い，2年間経過観察する．なお，ツベルクリン皮内反応陽性は結核菌感染のみならず，BCG接種や非結核性抗酸菌感染でもみられ，逆に，活動性結核の約25%は陰性である．陰性は真の陰性（結核菌未感染）や偽陰性（結核菌既感染にもかかわらず，陰性）を包含し，偽陰性として，栄養障害，高齢者，免疫疾患，リンパ系悪性腫瘍，副腎皮質ステロイド薬療法，慢性腎不全，サルコイドーシス，HIV感染者（AIDSを含む）や重症結核（播種性）等がある．従って，ツベルクリン皮内反応は結核の補助診断である．ツベルクリン皮内反応陽性は感染防御の指標とならないことも留意する．

【予防法－消毒・滅菌法－】(表3)

結核の予防ワクチンとして，弱毒ウシ型結核菌由来生ワクチンのBCGが汎用されている．乳幼児におけるBCG接種は有効とされているが，成人への効果は疑問視されている．結核菌を扱う業務に従事する前には，結核菌既感染の有無を確認しておくことが望ましい．確認にツベルクリン皮内反応，特に，結核菌特異抗原による末梢血単核細胞interferon-γ遊離試験が推奨される．予防内服にはイソニアジド（INH）が投与される．感染を受けたと判断される場合，INH300 mgを1日量として6～9ケ月投与する．感染結核菌がINH耐性の場合，リファンピシン（RIF）を投与する．

結核菌は熱湯による煮沸10分間で完全に殺菌できるが，オートクレーブ（121℃，30分）による滅菌が最も望ましい．消毒薬ではアルコール類，フェノール類，アルデヒド類が有効である．滅菌不可能な器具はグルタールアルデヒドに30分以上浸して消毒する．　**［大原直也・小林和夫］**

◉文献

1) 泉孝英監修，冨岡洋海編：結核（第4版），医学書院，2006.
2) 光山正雄編：結核，医薬ジャーナル社，2001.
3) 小林和夫：マイコバクテリウム（抗酸菌）と感染症，山西弘一監修，平松啓一・中込　治編，標準微生物学（第9版），pp279-292，医学書院，2005.
4) 露口泉夫編：最新医学別冊 新しい診断と治療のABC 41/呼吸器6 結核・非結核性抗酸菌症，最新医学社，2006.
5) 四元秀毅・山岸文雄：医療者のための結核の知識（第2版），医学書院，2005.
6) Morens D M et al: *Nature* **430**: 242-249, 2004.
7) Stop TB Partnership. http://www.stoptb.org/
8) 厚生労働省，平成18年結核発生動向調査年報集計結

果. http://www.mhlw.go.jp/bunya/kenkou/kekkaku-kansenshou03/06.html
9) World Health Organization. Tuberculosis. http://www.who.int/mediacentre/factsheets/fs104/en/index.html
10) エイズ予防情報ネット http://api-net.jfap.or.jp/
11) 厚生労働省. 結核・感染症に関する情報. http://www.mhlw.go.jp/bunya/kenkou/kekkaku-kansenshou.html
12) Centers for Disease Control and Prevention. TB guidelines. Infection contrl. http://www.cdc.gov/tb/pubs/mmwr/Maj_guide/infectioncontrol.htm

COLUMN **多剤耐性結核菌（MDR-TB）と超多剤耐性結核菌（XDR-TB）**

結核菌においても抗微生物薬耐性が問題となっているが，薬剤耐性結核菌で，INH と RIF に同時耐性菌を多剤耐性結核菌（Multidrug-resistant TB：MDR-TB），多剤耐性結核菌でフルオロキノロン耐性，かつカナマイシン，アミカシン，カプレオマイシン等，注射可能薬の少なくとも 1 剤以上に耐性の菌を超多剤耐性結核菌（Extensively drug-resistant TB：XDR-TB）という．薬剤耐性，特に，XDR-TB は抗結核化学療法がほとんど無効であり，生命予後も不良である．薬剤耐性結核菌に有効な新規抗結核薬の開発が希求されている．

Oral Microbiology Immunology 2008: 23: 413–418
Printed in Singapore. All rights reserved

ORAL MICROBIOLOGY
AND IMMUNOLOGY

Proteome analysis of *Porphyromonas gingivalis* cells placed in a subcutaneous chamber of mice

M. Yoshimura[1,4], N. Ohara[1,5], Y. Kondo[1], M. Shoji[1], S. Okano[2], Y. Nakano[3], Y. Abiko[2], K. Nakayama[1]

[1]Division of Microbiology and Oral Infection, Department of Molecular Microbiology and Immunology, Nagasaki University Graduate School of Biomedical Sciences, Nagasaki, Japan, [2]Department of Biochemistry and Molecular Biology, Nihon University School of Dentistry at Matsudo, Chiba, Japan, [3]Department of Preventive Dentistry, Kyushu University Faculty of Dental Science, Fukuoka, Japan

Yoshimura M, Ohara N, Kondo Y, Shoji M, Okano S, Nakano Y, Abiko Y, Nakayama K. Proteome analysis of Porphyromonas gingivalis *cells placed in a subcutaneous chamber of mice.*
Oral Microbiol Immunol 2008: 23: 413–418. © 2008 The Authors. Journal compilation © 2008 Blackwell Munksgaard.

Introduction: *Porphyromonas gingivalis*, an oral anaerobic bacterium, is considered a major pathogen for chronic periodontitis. Pathogenic bacteria usually upregulate or downregulate gene expression to combat the protective responses of their hosts.
Methods: To determine what protein is regulated when *P. gingivalis* cells invade host tissues, we analyzed the proteome of *P. gingivalis* cells that were placed in a mouse subcutaneous chamber by two-dimensional gel electrophoresis and mass spectrometry.
Results: Fourteen proteins were upregulated, while four proteins were downregulated. We focused on three upregulated proteins, PG1089 (DNA-binding response regulator RprY), PG1385 (TPR domain protein), and PG2102 (immunoreactive 61-kDa antigen), and constructed mutant strains that were defective in these proteins. Mouse abscess model experiments revealed that the mutant strain defective in PG1385 was clearly less virulent than the wild-type parent strain.
Conclusion: These results indicate that the PG1385 protein is involved in *P. gingivalis* virulence and that the method used here is useful when investigating the *P. gingivalis* proteins responsible for virulence.

Key words: *Porphyromonas gingivalis*; proteomics; subcutaneous chamber; virulence

Koji Nakayama, Division of Microbiology and Oral Infection, Department of Molecular Microbiology and Immunology, Nagasaki University Graduate School of Biomedical Sciences, Sakamoto 1-7-1, Nagasaki 852-8588, Japan
Tel.: +81 95 819 7648;
fax: +81 95 819 7650;
e-mail: knak@nagasaki-u.ac.jp
Accepted for publication January 25, 2008

[4]Present address: Department of Host Defense, Osaka City University Graduate School of Medicine, 1-4-3 Asahi-machi, Abeno-ku, Osaka 545-8585, Japan

[5]Present address: Department of Immunology, National Institute of Infectious Diseases, 1-23-1 Toyama, Shinguku-ku, Tokyo 162-8640, Japan

Periodontal diseases are the most prevalent of the oral inflammatory diseases characterized by the destruction of alveolar bone and the supporting connective tissue surrounding teeth (1, 23, 24). These destructive diseases are the outcome of a complex network of molecular and cellular interactions. At the boundary of the microbe and host compartments, many microbial virulence factors are produced to counter the actions of innate and acquired immunity by the host. The molecular activities of these microbes in the confines of a host remain to be determined so understanding the host–microbe interplay would be important to finding potential new targets to inhibit the activities or growth of the organisms responsible for periodontal diseases.

While a large number of different species have been recognized as members of the periodontal environment, *Porphyromonas gingivalis*, a gram-negative anaerobe, has long been considered to play an important role in initiation and progression of periodontal disease (25). The presence of this organism, acting either alone or as a mixed infection with other bacteria, and possibly in concert with certain immunological deficiencies in the host, appears to be essential for disease activity (7, 23). *P. gingivalis* is found to express numerous potential virulence factors, such as fimbriae, hemagglutinins, lipopolysaccharides, and various proteases that are capable of hydrolyzing collagen, immunoglobulins,

iron-binding proteins, and complement factors (8, 11). Expression of these virulent factors is thought to be tightly regulated in response to environmental cues. Although a number of studies describe gene expression of *P. gingivalis* being regulated by environmental stresses (3, 9, 14, 16, 19, 21, 26), gene expression of *P. gingivalis* cells in *in vivo* lesions is not completely understood.

In 1991, Genco et al. (5) reported the development of a mouse subcutaneous chamber model that allows the assessment of host–parasite interactions in localized infections. Burns et al. (2) have shown using the subcutaneous chamber model that the cytokine response to live *P. gingivalis* is impaired in mice that are deficient for Toll-like receptor 2 (TLR-2), but not in TLR-4-deficient mice, and that *P. gingivalis* survival in chamber exudates and blood decreased in TLR-2-deficient mice more than in the wild-type and TLR-4-deficient mice, suggesting that induction of cytokines including tumour necrosis factor-α, interleukin-1β, interferon-γ, and interleukin-10 may not contribute to *P. gingivalis* clearance and rather interferes with it in the subcutaneous chamber model. They also found that the degree of alveolar bone loss in the TLR-2-deficient mice is less than that in the wild-type mice in *P. gingivalis* oral infection experiments.

Using this chamber model, one can easily sample bacteria grown *in vivo* and assess the modulation of potential virulence factors by this specific growth environment. In this study, we describe the identification of genes whose products are upregulated or downregulated in the host using two-dimensional (2D) gel electrophoresis; this can be used to identify changes in gene expression caused by stress treatments and growth conditions. Further, we constructed *P. gingivalis* mutants that were defective in the genes encoding those proteins that were upregulated in the mouse subcutaneous chamber. We also compared the virulence of these mutants using the mouse subcutaneous abscess model.

Materials and methods

Bacterial strain and growth conditions

Porphyromonas gingivalis strain W83 was grown anaerobically (10% CO_2, 10% H_2, 80% N_2) in enriched brain–heart infusion (BHI) broth as described previously (12). Bacterial cells were grown at 37°C until an optical density at 550 nm (OD_{550}) of 1.0 was reached. Cultures were then concentrated by centrifugation at 10,000 ***g*** for 10 min and cells were either collected (control sample), or resuspended in 1/30 of the original volume in fresh, enriched BHI broth.

Experimental animals

Female BALB/c mice approximately 8 weeks old were used in these studies. Coil-shaped subcutaneous chambers were prepared and surgically implanted as previously described by Genco et al. (5). One week after implantation, the chambers were inoculated with 0.4 ml of a concentrated suspension of *P. gingivalis* in enriched BHI broth. Six hours after inoculation, chamber fluid containing bacterial cells (*in vivo* sample) was aseptically removed from each implanted chamber using a hypodermic needle (25-gauge) and syringe. Usually, chamber fluid harvested from three mice was mixed and subjected to 2D gel electrophoresis.

2D gel electrophoresis

P. gingivalis cells were dissolved in 10% trichloroacetic acid. The resulting precipitates were washed several times with acetone and dried. The cells were then suspended in a lyzing buffer [7 M urea, 2 M thiourea, 4% 3-((3-cholamidopropyl)dimethylammonio)-1-propanesulfonic acid (CHAPS), 1 mM ethylenediaminetetraacetic acid (EDTA), 2 mM tributylphosphin, and 40 mM Tris base]. The lysates were sonicated and centrifuged at 15,000 ***g*** for 10 min. After centrifugation, the supernatants were subjected to 2D gel analysis. Proteins (200 μg) were separated in the first dimension by isoelectric focusing using the Multiphor II system (GE Healthcare Biosciences, Waukesha, WI) according to the manufacturer's instructions. Each protein of the same concentration was loaded on 18-cm rehydrated isoelectric focusing strips with an immobilized pH gradient between pH 4 and 7 (GE Healthcare Biosciences). Proteins were then electrofocused at 20°C in four stages. Focused gel strips were equilibrated for 10 min in equilibration solution A [50 mM Tris–HCl (pH 8.8), 30% glycerol, 6 M urea, 2% sodium dodecyl sulfate (SDS), and 40 mM dithiothreitol) and for further 10 min in equilibration solution B [50 mM Tris–HCl (pH 8.8), 30% glycerol, 6 M urea, 2% SDS, and 135 mM iodoacetamide). SDS–polyacrylamide gel electrophoresis was then performed using 12% separating gels, according to the manufacturer's instructions. After electrophoresis, proteins in the gels were stained with Coomassie brilliant blue R-250.

Peptide mass fingerprinting

Protein spots that differed in their expression profiles were semi-automatically extracted, digested with trypsin, and purified using a ProteomIQ Xcise In-Gel Digest kit (Proteome Systems Inc., Sydney, Australia) and a high-throughput gel-excise processor (Xcise; Shimadzu Co., Kyoto, Japan). Peptide mass analyses were performed using an AXIMA CFR (Shimadzu Co.) matrix-assisted laser desorption ionization time of flight (MALDI-TOF) mass spectrometer in reflectron mode.

Protein identification

Amino acid sequences of the *P. gingivalis* W83 proteins were obtained from The Institute for Genomic Research website (http://www.tigr.org). Proteins were identified from peptide mass data using the database search engine (MASCOT; Matrix Science Ltd, London, UK). The MASCOT score is the probability score for the peptide match calculated from the amino acid sequences database based on the Mowse scoring algorithm (15).

Construction of *P. gingivalis* mutants

P. gingivalis W83 genome sequence data were obtained from The Institute for Genomic Research website (http://www.tigr.org). *P. gingivalis rprY* mutants were constructed as follows. A DNA fragment corresponding to a 0.73-kilobase (kb) region within the *rprY* gene upper region was generated by polymerase chain reaction (PCR) using *P. gingivalis* W83 chromosomal DNA as the template with a forward primer, 5′-GGGTACCCA-AAGCATTGATTCCGTTTGC, containing a *Kpn*I site (underlined) and a backward primer, 5′-GGAATTCCCCC-TCTTCTCCATCACCAGA, containing an *Eco*RI site (underlined). The resulting fragment was cloned into the pGEM-T Easy Vector (Promega, Madison, WI), to yield pKD714. A DNA fragment corresponding to a region (0.50-kb) located in the *rprY* gene lower region was obtained by PCR with a forward primer, 5′-GGG-ATCCCATGATGCCACGTAAGGATGG, containing a *Bam*HI site (underlined) and a backward primer, 5′-GGCGGCCGCCGC-CCTTTCCGTGGATATTCT, containing a *Not*I site (underlined). The resulting fragment was cloned into the pGEM-T Easy Vector to yield pKD715. The *Kpn*I–*Eco*RI region of pKD714 containing the 0.73-kb fragment was inserted into the same sites of pBluescript SK-, resulting in pKD716.

The *Sac*II–*Sac*I fragment (unique sites of the pGEM-T Easy Vector) of pKD715 containing the *rprY* lower region was inserted with the same sites of pKD716, yielding pKD717. To generate a non-polar mutant, the *erm*F DNA block (1.0-kb), which contains the putative promoter and ribosome binding site but not the terminator region, was generated by PCR using pKD399 (22) as the template with a forward primer, 5′-GGGATCCCCCGATAGCTTCCGCTAT, containing a *Bam*HI site (underlined) and a backward primer, GGATCCCCTACGAAGGATGAAATTT, containing a *Bam*HI site (underlined). The resulting fragment was cloned into the pGEM-T Easy Vector to yield pKD718. To generate an insertion mutant or a non-polar mutant, the *erm*F–*erm*AM DNA block (2.1-kb) from pKD399 or the *erm*F DNA block (1.0-kb) from pKD718 was inserted into the *Bam*HI site of pKD717 that was located at the junction of the 0.73-kb *rprY*-upstream fragment and the 0.60-kb *rprY*-downstream fragment to yield pKD719 or pKD720. The orientation of the *erm*F–*erm*AM DNA block of pKD719 was opposite to that of the *rprY* gene, whereas the orientation of the *erm*F DNA block of pKD720 was the same as that of the *rprY* gene. The pKD719 or pKD720 plasmid DNA was linearized by *Fsp*I digestion and introduced into cells of *P. gingivalis* W83 by electroporation. The cells were spread on tryptic soy (TS) agar containing 10 μg/ml erythromycin (Em) and incubated anaerobically for 7 days. Em-resistant transformants (KDP156 and KDP157) were obtained after the above procedure with pKD719 and pKD720, respectively. Proper DNA replacement of these transformants was verified by Southern blot analysis.

The *P. gingivalis* PG2102 insertion mutant was constructed as follows. A DNA fragment corresponding to a region (0.62-kb) within the PG2102 gene upper region was generated by PCR using *P. gingivalis* W83 chromosomal DNA as the template with a forward primer, 5′-GGGTACCCCGGCAATAGCAATGTGAAGA, containing a *Kpn*I site (underlined) and a backward primer, 5′-GGAATTCCCCACTGAAATTCGGGATCAT, containing an *Eco*RI site (underlined). The resulting fragment was cloned into the pGEM-T Easy Vector (Promega), to yield pKD721. A DNA fragment corresponding to a region (0.64-kb) located in the PG2102 gene lower region was obtained by PCR with a forward primer, 5′-GGGATCCCACGATCAATGGGGAGAGTTG, containing a *Bam*HI site (underlined) and a backward primer, GGCGGCCGCCTGCACGTTCAGCCTGTATTC, containing a *Not*I site (underlined). The resulting fragment was cloned into the pGEM-T Easy Vector to yield pKD722. The *Kpn*I–*Eco*RI region of pKD721 containing the 0.62-kb fragment was inserted into the same sites of pBluescript SK-, resulting in pKD723. The *Bam*HI–*Not*I fragment of pKD722 containing the PG2102 lower region was inserted with the same sites of pKD723, yielding pKD724. The *erm*F–*erm*AM DNA block (2.1-kb) from pKD399 was inserted in the *Eco*RI–*Bam*HI site of pKD717, which was located at the junction of the 0.62-kb PG2102-upstream fragment and the 0.64-kb PG2102-downstream fragment to yield pKD725. The pKD725 plasmid DNA was linearized by *Not*I digestion and introduced into cells of *P. gingivalis* W83 by electroporation. Proper DNA replacement of the resulting Em-resistant transformant (KDP158) was verified by Southern blot analysis.

The *P. gingivalis* PG1385 insertion mutant was constructed as follows. A DNA fragment corresponding to a region (1.17-kb) within the PG1385 gene was generated by PCR using *P. gingivalis* W83 chromosomal DNA as the template with a forward primer, 5′-CCTGTTTGCAGCAGTTATGC and a backward primer, 5′-TTTCCTTCGTGACGCTCTGT. The resulting fragment was cloned into the pGEM-T Easy Vector (Promega), to yield pKD726. The *erm*F–*erm*AM DNA block (2.1-kb) from pKD399 was inserted in the *Bgl*II site of pKD726 to yield pKD727. The pKD727 plasmid DNA was linearized by *Fsp*I digestion and introduced into cells of *P. gingivalis* W83 by electroporation. Proper DNA replacement of the resulting Em-resistant transformant (KDP159) was verified by Southern blot analysis.

Mouse subcutaneous abscess model assay

Virulence of *P. gingivalis* strains W83, KDP157, KDP158 and KDP159 was determined as described by Neiders et al. (13). Each bacterial strain was grown in enriched BHI broth to an OD_{550} of 1.0. The cells were harvested, resuspended, and adjusted to a concentration of 1×10^{11} colony-forming units/ml in the same medium. Female BALB/c mice (8–10 weeks old) were challenged with subcutaneous injections of 0.1 ml bacterial suspension at two sites on the depilated dorsal surface (0.2 ml per mouse). Injected mice were examined daily for the presence and locations of secondary lesions and the health status of each mouse was recorded.

Statistical analysis

Statistical analysis was by two-way repeated measures analysis of variance (ANOVA) for comparison of the survival and one-way ANOVA for comparison of the virulence between wild-type and mutant strains. Tukey's honestly significant differences (HSD) test was used as a *post hoc* test. A difference with $P < 0.05$ was considered significant. All statistical analyses were performed using the STATISTICAL ANALYSIS SYSTEM (Version 14.0, SPSS Japan Inc., Tokyo, Japan). Student's *t*-test was used to evaluate the difference in the mean value of abscess formation rate of three experiments.

Results

Proteome analysis

We attempted to compare the protein expression in the *in vivo* sample with that in the control sample. Two representative 2D separations of cellular proteins obtained from the control sample and *in vivo* sample are presented in Fig. 1A and Fig. 1B, respectively. Fourteen protein spots of the *in vivo* sample were markedly increased, and four spots were decreased compared to those of the control sample (Fig. 1). Next, the peptide mass analysis of these proteins and database analysis with the *P. gingivalis* genome sequence were performed (Table 1). Of the 14 upregulated proteins examined, 10 proteins were identified as *P. gingivalis* proteins. Four proteins were not determined or were derived from mouse. We found that the upregulated-proteins were related to protein synthesis, detoxification, energy metabolism, and degradation of proteins. Interestingly, heat-shock protein DnaK was found to be downregulated in the *in vivo* sample.

Virulence of *P. gingivalis* mutants in the mouse subcutaneous abscess model

From the protein list given in Table 1, three upregulated proteins, PG1089 (RprY), PG2102 (immunoreactive 61-kDa antigen), and PG1385 [tetratricopeptide repeat (TPR) domain protein], were selected, and chromosomal mutants defective in the proteins were constructed to analyze the involvement of these proteins in *P. gingivalis* virulence. BALB/c mice were challenged with subcutaneous injections of bacterial suspensions of strain W83 and its mutant strains, KDP157, KDP158, and KDP159 (2×10^{10} colony-forming units per animal). The wild-type

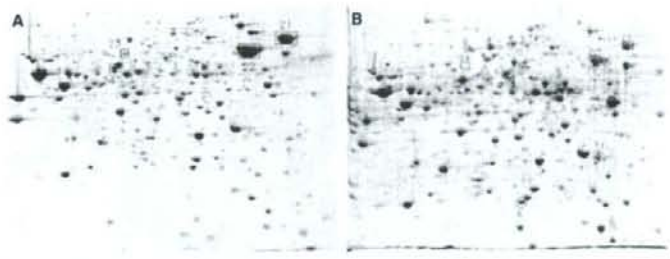

Fig. 1. Representative two-dimensional electrophoresis gels of the *Porphyromonas gingivalis* cell preparation. (A) *P. gingivalis* cells grown in enriched brain–heart infusion broth. (B) *P. gingivalis* cells placed in a mouse subcutaneous chamber for 6 h. Experiments were performed more than three times. The averaged gels were examined using image matching software (PDQUEST Version 7.2; Bio-Rad, Hercules, CA) to detect spots. Spots were analyzed with MALDI-TOF mass spectrometry. The identified proteins are listed in Table 1. The upregulated protein spots are numbered from 1 to 14 and the downregulated protein spots are numbered from 21 to 24.

Table 1. Identification of protein spots with MALDI-TOF mass analysis

Spot no.[1]	TIGR locus	Definition	MASCOT score[2]
Upregulated			
1	PG0387	Translation elongation factor Tu	122
2	–	Not determined	
3	–	Actin from the host	
4	PG1055	Thiol protease	156
5	PG1360	Phosphoribosylamine-glycine ligase	58
6	PG0618	Alkyl hydroperoxide reductase, C subunit	105
7	PG1424	Peptidylarginine deiminase	110
8	–	A serum protein from the host	
9	PG0249	Oxaloacetate decarboxylase, putative	65
10	PG1844	Lysine-specific cysteine proteinase Kgp	70
11	–	Not determined	
12	PG2102	Immunoreactive 61-kDa antigen PG91	145
13	PG1089	DNA-binding response regulator RprY	167
14	PG1385	TPR domain protein	204
Downregulated			
21	PG1208	DnaK protein	58
22	PG0520	Chaperonin, 60-kDa	92
23	PG0962	Prolyl-tRNA synthetase	107
24	PG0690	4-Hydroxybutyrate coenzyme A-transferase	48

[1]The protein spots indicated in Fig. 1 were analyzed using matrix-assisted laser desorption ionization time of flight (MALDI-TOF) mass spectrometry.
[2]Proteins were identified using MASCOT with a custom *P. gingivalis* W83 open reading frame database obtained from The Institute for Genomic Research (TIGR).
TPR, tetratricopeptide repeat.

strain W83 induced spreading, ulcerative lesions on the abdomens of all mice tested by 24 h and the mice showed ruffled hair, whereas the mice injected with KDP159 displayed fewer lesions with regard to the number of mice with lesions, the size of the abscess, and the whole body state (Fig. 2). The average abscess sizes for the mice injected with KDP157 and KDP158 were smaller than that for the mice injected with W83, and the whole body state of the mice injected with KDP157 was better than that of the mice injected with W83; however, there were no statistical differences in the number of mice with lesions and the size of abscess.

Discussion

In the present study, we used 2D electrophoresis technology to study host–microbe interactions. 2D electrophoresis is a powerful tool for resolving protein mixtures into their component polypeptides and can be used to compare different test samples. It is reported that 2D electrophoresis of proteins extracted from *P. gingivalis* often gave poor resolution and/or the disappearance of certain protein spots as a result of the presence of abundant proteases within the samples. However, degradation of proteins could be prevented by pretreatment of cells with trichloroacetic acid as previously described by Pridmore et al. (17).

P. gingivalis strain W83 was selected as the virulent strain because many previous reports have described its virulence-associated activities and disease-promoting characteristics *in vitro* and *in vivo* (6, 10). When the strain was directly inoculated into the subcutaneous tissues of mice, this inoculation resulted in rapidly spreading purulent infection. We, therefore, tried to use the subcutaneous chamber model to obtain sufficient samples of *in vivo*-grown bacterial cells.

Ten proteins, the amounts of which were increased *in vivo*, included proteins with various functions such as oxidative stress protection and protein degradation. In this study, we focused on three proteins [immunoreactive 61-kDa antigen (PG2102), DNA-binding response regulator RprY (PG1089), and TPR domain protein (PG1385)] and constructed mutant strains that were defective in these proteins. These mutant strains formed pigmented colonies on the blood agar plates and produced gingipains as well as the wild-type parent strain (data not shown). Virulence analysis with subcutaneous injection in mice revealed that the PG1385-defective mutant was less virulent than the wild-type parent strain, whereas we could not find statistical differences in the number of mice with lesions and the size of abscess among the PG2102-defective mutant, the PG1089-defective mutant, and the wild-type parent strain. However, the whole body state of the mice injected with the PG1089-defective mutant was obviously better than that of the mice injected with the wild-type parent strain.

PG1385 is one of the TPR-containing proteins. TPR is a structural motif present in a wide range of proteins. It mediates a variety of different protein–protein interactions. TPR-containing proteins are found in a number of different organisms including prokaryotes and eukaryotes. Okano et al. (14) reported that 19 proteins of *P. gingivalis* W83 are upregulated by aeration and that the 19 proteins include HtpG (PG0045), chaperonin 60-kDa (PG0520), DnaK (PG1208), TPR domain protein (PG1385), trigger factor (PG0762), RagA (PG0185), and AhpC (PG0618). In the subcutaneous chamber in the present study, TPR domain protein (PG1385) and AhpC (PG0618) were increased, whereas chaperonin 60-kDa (PG0520) and DnaK (PG1208) were decreased, indicating that oxidative stress is among the stresses suffered by *P. gingivalis* cells in the chamber. The TPR domain protein

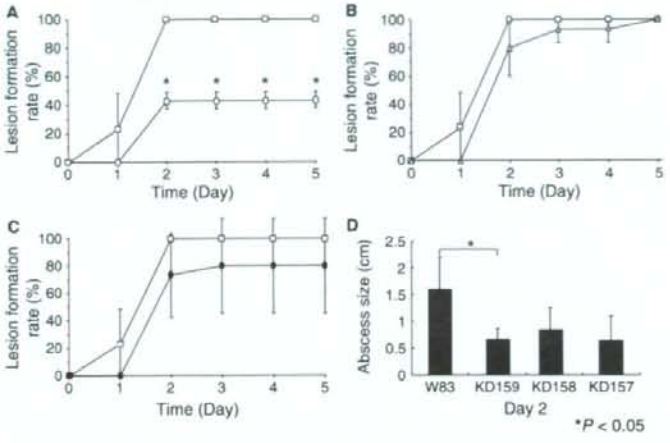

Fig. 2. Mouse subcutaneous abscess model assay. *Porphyromonas gingivalis* cells were subcutaneously injected at two sites on the depilated dorsal surface of female BALB/c mice. The animal experiments used six mice for each bacterial strain and were performed three times. (A–C) Lesion formation rates: (A) open rectangle, W83; open triangle, KDP159 (PG1385 mutant); (B) open rectangle, W83; open circle, KDP158 (PG2102 mutant); (C) open rectangle, W83; closed circle, KDP157 (PG1089 mutant). (D) Average diameter of abscesses on the abdomens 2 days after inoculation.

(PG1385) is a major protein located in the periplasm (20), implying that PG1385 binds to other proteins in the periplasm or protruding from the inner or outer membrane.

PG1089 is a feature of the DNA-binding response regulator of the two-component system and its homologue, RprY, is found in *Bacteroides fragilis*. The *B. fragilis rprY* gene is located downstream of *rprX*, which encodes one of the histidine protein kinase components of the two-component regulatory system (18). However, there is no such a gene encoding the histidine protein kinase around PG1089 in the *P. gingivalis* genome. Expression of *B. fragilis rprX* and *rprY* genes in *Escherichia coli* downregulates the outer membrane porin proteins OmpF and OmpC, suggesting that the two-component system regulates the expression of outer membrane proteins (18). It was reported that the gene encoding PG1089 is induced during contact of *P. gingivalis* cells with Hep-2 epithelial cells (9). Very recently, Duran-Pinedo et al. (4) have found that RprY directly binds and upregulates the *ahpC* gene as well as the NADH : ubiquinone oxidoreductase operon.

In conclusion, we found 10 up-regulated genes and 4 down-regulated genes by proteomics analysis of *P. gingivalis* cells placed in a mouse subcutaneous chamber. Mutant analysis of the up-regulated genes suggested that the PG1385-encoding gene was clearly responsible for virulence of *P. gingivalis*.

Acknowledgment

This study was supported by Grants-in-Aid (no. 18018032 and no. 17209057) from the Ministry of Education, Culture, Sports, Science, and Technology.

References

1. Armitage GC. Periodontal diseases: diagnosis. Ann Periodontol 1996: **1**: 37–215.
2. Burns E, Bachrach G, Shapira L, Nussbaum G. TLR2 is required for innate response to *Porphyromonas gingivalis*: activation leads to bacterial persistence and TLR2 deficiency attenuates induced alveolar bone resorption. J Immunol 2006: **177**: 8296–8300.
3. Diaz PI, Slakeski N, Reynolds EC, Morona R, Rogers AH, Kolenbrander PE. Role of *oxyR* in the oral anaerobe *Porphyromonas gingivalis*. J Bacteriol 2006: **188**: 2454–2462.
4. Duran-Pinedo A, Nishikawa EK, Duncan MJ. The RprY response regulator of *Porphyromonas gingivalis*. Mol Microbiol 2007: **64**: 1061–1074.
5. Genco CA, Cutler CW, Kapczynski D, Maloney K, Arnold RR. A novel mouse model to study the virulence of and host response to *Porphyromonas* (*Bacteroides*) *gingivalis*. Infect Immun 1991: **59**: 1255–1263.
6. Grenier D, Mayrand D. Selected characteristics of pathogenic and nonpathogenic strains of *Bacteroides gingivalis*. J Clin Microbiol 1987: **25**: 738–740.
7. Haffajee AD, Socransky SS. Microbial etiological agents of destructive periodontal diseases. Periodontol 2000 1994: **5**: 78–111.
8. Holt SC, Kesavalu L, Walker S, Genco CA. Virulence factors of *Porphyromonas gingivalis*. Periodontol 2000 1999: **20**: 168–238.
9. Hosogi Y, Duncan MJ. Gene expression in *Porphyromonas gingivalis* after contact with human epithelial cells. Infect Immun 2005: **73**: 2327–2335.
10. Laine ML, van Winkelhoff AJ. Virulence of six capsular serotypes of *Porphyromonas gingivalis* in a mouse model. Oral Microbiol Immunol 1998: **13**: 322–325.
11. Lamont RJ, Jenkinson HF. Life below the gum line: pathogenic mechanisms of *Porphyromonas gingivalis*. Microbiol Mol Biol Rev 1998: **62**: 1244–1263.
12. Nakayama K, Kadowaki T, Okamoto K, Yamamoto K. Construction and characterization of arginine-specific cysteine proteinase (Arg-gingipain)-deficient mutants of *Porphyromonas gingivalis*: evidence for significant contribution of Arg-gingipain to virulence. J Biol Chem 1995: **270**: 23619–23626.
13. Neiders ME, Chen PB, Suido H et al. Heterogeneity of virulence among strains of *Bacteroides gingivalis*. J Periodontal Res 1989: **24**: 192–198.
14. Okano S, Shibata Y, Shiroza T, Abiko Y. Proteomics-based analysis of a counter-oxidative stress system in *Porphyromonas gingivalis*. Proteomics 2006: **6**: 251–258.
15. Pappin DJ, Hojrup P, Bleasby AJ. Rapid identification of proteins by peptide-mass fingerprinting. Curr Biol 1993: **3**: 327–332.
16. Park Y, Yilmaz O, Jung I, Lamont RJ. Identification of *Porphyromonas gingivalis* genes specifically expressed in human gingival epithelial cells by using differential display reverse transcription-PCR. Infect Immun 2004: **72**: 3752–3758.
17. Pridmore AM, Devine DA, Bonass WA, Silley P. Influence of sample preparation technique on two-dimensional gel electrophoresis of proteins from *Porphyromonas gingivalis*. Lett Appl Microbiol 1999: **28**: 245–249.
18. Rasmussen BA, Kovacs E. Cloning and identification of a two-component signal-transducing regulatory system from *Bacteroides fragilis*. Mol Microbiol 1993: **7**: 765–776.
19. Rodrigues PH, Progulske-Fox A. Gene expression profile analysis of *Porphyromonas gingivalis* during invasion of human coronary artery endothelial cells. Infect Immun 2005: **73**: 6169–6173.
20. Seers CA, Slakeski N, Veith PD et al. The RgpB C-terminal domain has a role on attachment of RgpB to the outer membrane and belongs to a novel C-terminal-domain family found in *Porphyromonas gingivalis*. J Bacteriol 2006: **188**: 6376–6386.
21. Shelburne CE, Gleason RM, Germaine GR et al. Quantitative reverse transcription polymerase chain reaction analysis of

Porphyromonas gingivalis gene expression *in vivo*. J Microbiol Meth 2002: **49**: 147–156.
22. Shoji M, Naito M, Yukitake H et al. The major structural components of two cell surface filaments of *Porphyromonas gingivalis* are matured through lipoprotein precursors. Mol Microbiol 2004: **52**: 1513–1525.
23. Socransky SS, Haffajee AD. The bacterial etiology of destructive periodontal disease: current concepts. J Periodontol 1992: **63**: 322–331.
24. Williams RC. Periodontal disease. N Engl J Med 1990: **322**: 373–382.
25. Zambon JJ, Reynolds HS, Slots J. Black-pigmented *Bacteroides* spp. in the human oral cavity. Infect Immun 1981: **32**: 198–203.
26. Zhang Y, Wang T, Chen W et al. Differential protein expression by *Porphyromonas gingivalis* in response to secreted epithelial cell components. Proteomics 2005: **5**: 198–211.

DNA Research 15, 215–225, (2008) doi:10.1093/dnares/dsn013

Determination of the Genome Sequence of *Porphyromonas gingivalis* Strain ATCC 33277 and Genomic Comparison with Strain W83 Revealed Extensive Genome Rearrangements in *P. gingivalis*

Mariko Naito[1], Hideki Hirakawa[2], Atsushi Yamashita[3], Naoya Ohara[1,†], Mikio Shoji[1], Hideharu Yukitake[1], Keisuke Nakayama[4], Hidehiro Toh[3,‡], Fuminobu Yoshimura[5], Satoru Kuhara[6], Masahira Hattori[3,7], Tetsuya Hayashi[4], and Koji Nakayama[1,*]

Division of Microbiology and Oral Infection, Department of Molecular Microbiology and Immunology, Nagasaki University Graduate School of Biomedical Sciences, Sakamoto 1-7-1, Nagasaki 852-8588, Japan[1]; Graduate School of Systems Life Sciences, Kyushu University, Hakozaki 6-10-1, Higashi-ku, Fukuoka 812-8581, Japan[2]; Kitasato Institute for Life Sciences, Kitasato University, Kitasato 1-15-1, Sagamihara, Kanagawa 228-8555, Japan[3]; Division of Bioenvironmental Science, Frontier Science Research Center, University of Miyazaki, Kihara 5200, Kiyotake, Miyazaki 889-1692, Japan[4]; Department of Microbiology, School of Dentistry, Aichi-Gakuin University, 1-100 Kusumoto-cho, Chikusa-ku, Nagoya 464-8650, Japan[5]; Graduate School of Genetic Resources Technology, Kyushu University, Hakozaki 6-10-1, Higashi-ku, Fukuoka 812-8581, Japan[6] and Department of Computational Biology, Graduate School of Frontier Sciences, The University of Tokyo, Kashiwanoha 5-1-5, Chiba 277-8561, Japan[7]

(Received 10 March 2008; accepted on 13 May 2008; published online 3 June 2008)

Abstract

The gram-negative anaerobic bacterium *Porphyromonas gingivalis* is a major causative agent of chronic periodontitis. *Porphyromonas gingivalis* strains have been classified into virulent and less-virulent strains by mouse subcutaneous soft tissue abscess model analysis. Here, we present the whole genome sequence of *P. gingivalis* ATCC 33277, which is classified as a less-virulent strain. We identified 2090 protein-coding sequences (CDSs), 4 RNA operons, and 53 tRNA genes in the ATCC 33277 genome. By genomic comparison with the virulent strain W83, we identified 461 ATCC 33277-specific and 415 W83-specific CDSs. Extensive genomic rearrangements were observed between the two strains: 175 regions in which genomic rearrangements have occurred were identified. Thirty-five of those genomic rearrangements were inversion or translocation and 140 were simple insertion, deletion, or replacement. Both strains contained large numbers of mobile elements, such as insertion sequences, miniature inverted-repeat transposable elements (MITEs), and conjugative transposons, which are frequently associated with genomic rearrangements. These findings indicate that the mobile genetic elements have been deeply involved in the extensive genome rearrangement of *P. gingivalis* and the occurrence of many of the strain-specific CDSs. We also describe here a very unique feature of MITE400, which we renamed MITE*PgRS* (MITE of *P. gingivalis* with Repeating Sequences).

Key words: *Porphyromonas gingivalis*; whole genome sequence; genome rearrangement; conjugative transposon; MITE

1. Introduction

Periodontal disease, the major cause of tooth loss in the general populations of industrial nations,[1,2] is a chronic inflammatory disease of the periodontium that leads to erosion of the attachment apparatus

Edited by Katsumi Isono

† Present address: Department of Immunology, National Institute of Infectious Diseases, 1-23-1 Toyama, Shinjuku-ku, Tokyo 162-8640, Japan

‡ Present address: RIKEN Genomic Sciences Center, 1-7-22 Suehiro-cho, Tsurumi-ku, Yokohama 230-0045, Japan

* To whom correspondence should be addressed. Tel. +81 95-819-7649. Fax. +81 95-819-7650. E-mail: knak@nagasaki-u.ac.jp

and supporting bone for teeth[3] and is one of the most frequently occurring infectious diseases in humans.[4] Recently, a number of epidemiological studies have shown significant relationships between periodontal diseases and cardiovascular diseases.[5–8] Several periodontal pathogens, including *Porphyromonas gingivalis*, have been found in atherosclerotic plaques.[9,10]

Porphyromonas gingivalis is a gram-negative anaerobic bacterium that is classified in the genus *Porphyromonas*, family *Porphyromonadaceae*, order *Bacteroidales*, class *Bacteroides*, phylum *Bacteroidetes*.[11] The bacterium, which is often found in deep periodontal pockets of humans, is asaccharolytic and highly proteolytic. *Porphyromonas gingivalis* produces a broad array of potential virulence factors involved in tissue colonization and destruction as well as host defense perturbation. Potential virulence factors of *P. gingivalis* have been extensively described in several reviews.[12–14] Among these, fimbriae (FimA fimbriae and Mfa1 fimbriae), which are responsible for attachment of bacterial cells to host cell surfaces, and proteolytic enzymes such as Arg-gingipain (Rgp) and Lys-gingipain (Kgp), which degrade various host proteins, have been studied in detail.[15–17] However, no systematic analysis of *P. gingivalis* virulence factors has yet been carried out.

Using the mouse subcutaneous soft tissue abscess model, *P. gingivalis* strains are divided into virulent and less-virulent strains. Virulent strains such as W83 typically induce a necrotic lesion at the site of injection within 24 h. An extending gangrene-like necrosis spreads, secondarily along fascial planes into the abdominal and thoracic areas between 24 and 48 h, producing a foul-smelling and bloody exudate under the animal's skin. Sloughing and scab formation from necrosis of the epidermis, weight and hair loss, and animal death from microbial sepsis also are common clinical features. Less-virulent strains such as ATCC 33277 produce only a localized abscess 3 days after subcutaneous inoculation.[18] W83 has already been genome-sequenced.[19] Strain ATCC 33277 is the type strain of *P. gingivalis* and has been widely used for characterization of pathophysiological features of the microorganism. We have used molecular genetic techniques to study *P. gingivalis* and have constructed a number of mutants from strain ATCC 33277 to investigate the roles of various genes in the pathogenicity of *P. gingivalis*.[20–25] In the present study, we determined the whole genome sequence of strain ATCC 33277 and performed a genomic comparison of ATCC 33277 and W83. Our findings showed that extensive genome rearrangements have taken place between the two strains. Transposable elements appear to have played central roles in the generation of these genome rearrangements, which have in turn created many strain-specific genes, including several potentially virulence-related genes.

2. Materials and methods

2.1. Genome sequencing

Porphyromonas gingivalis ATCC 33277 was obtained from the American Type Culture Collection (ATCC) and has been kept for more than 20 years. *Porphyromonas gingivalis* W83 was obtained from Dr M. J. Duncan (Department of Molecular Genetics, The Forsyth Institute). *Porphyromonas gingivalis* GAI7802 was obtained from Dr E. Hoshino (Niigata University School of Dentistry), TDC60, TDC117, and TDC275 were obtained from Dr K. Ishihara (Tokyo Dental College), and SU63 was obtained from Dr M. Yoneda (Fukuoka Dental College). For preparing the genomic DNA, a single colony of each *P. gingivalis* strain was grown at 37°C anaerobically (10% CO_2, 10% H_2, 80% N_2) in brain heart infusion broth (BD Bioscience, San Jose, CA, USA) supplemented with 5 μg of hemin and 0.5 μg of menadione per ml.

The genomic DNA was randomly sheared by Hydroshear (GeneMachines) and used for genomic library construction. We prepared two pTS1-based random genomic libraries with insert sizes of 1–2 kb or ~10 kb. Sequencing was carried out using BigDye v3.1 chemistry on ABI 3700 or ABI 3730 sequencers (Applied Biosystems) or ET chemistry on MegaBACE 4500 sequencers (GE Healthcare). The whole genome sequence was obtained by assembling 36 394 reads (9.5-fold coverage) from both shotgun libraries. The Phred/Phrap software package[26] was used for base-calling, quality assessment, and sequence assembly. Assemblies were visualized for counting-based variations and detecting misassembly using Consed software.[27] Numbers and lengths of the *Not*I fragments of the ATCC 33277 chromosome predicted from the determined nucleotide sequence agreed well with those observed in pulsed field gel electrophoresis analysis of *Not*I-digested ATCC 33277 genomic DNA.[28]

2.2. Sequence analysis

Protein-coding sequences (CDSs) were identified by using the combination of GENOME GAMBLER v1.51,[29] CRITICA,[30] GENEHACKER,[31] and GLIMMER v2.0 programs.[32] The sequences of 3′ terminal regions of all 16S ribosomal RNA genes in W83, and ATCC 33277 were identical to that of *Bacteroides fragilis* (AGAAAGGAGG, the accession number M61006). Each CDS was thus reviewed manually for the presence of a start codon (ATG, TTG, or GTG) and a potential ribosome-binding sequence that should be

related to a part of the AGAAAGGAGG sequence. Functional annotation of the CDSs was made on the basis of results of homology searches against public protein (nr) database from NCBI (http://www.ncbi.nlm.nih.gov/) by the BLASTP program.[33] tRNA genes were identified by the tRNAscan-SE program.[34] All-to-all BLASTP analysis of CDSs was performed between W83 and ATCC 33277 to identify conserved and strain-specific CDSs. Since each genome contained a number of multi-copied CDSs such as transposase genes, we first grouped these multi-copied CDSs in each genome using BLASTCLUST[33] (The threshold used was $\geq$90% amino-acid sequence identity.). The largest CDS in each multi-copied CDS group was used as the representative of each group for the identification of conserved and strain-specific CDSs. In the present study, we defined conserved CDSs as ones that had 60–140% of the length of a query sequence and showed $\geq$90% sequence identity in bidirectional best-hit analysis. The MUMmer program[35] was used to define conserved genomic regions, inversions, and translocations between the two genomes. The Pip Maker program[36] was also used for DNA sequence alignment.

2.3. *PCR analysis*

The total genomic DNA of ATCC 33277 and two pairs of PCR primers (CTnPg1-left and CTnPg1-right, CTnPg1-up and CTnPg1-down, Supplementary Table S1) were used to detect the excision of a conjugative transposon (CTn), CTnPg1. These primer pairs were designed to amplify the *attP* and *attB* regions for CTnPg1, respectively. PCR amplification was performed by using 100 ng of the genomic DNA and *LA Taq* (Takara Shuzo, Tokyo, Japan) in the following setting: preheating (94°C for 1 min) and 30 cycles of DNA denaturation (94°C for 20 s), primer annealing (55°C for 30 s) and DNA extension (68°C for 2 min). The amplified fragments were subjected to direct sequencing to determine the nucleotide sequences of the *attP* and *attB* sites.

2.4. *RNA isolation and real-time PCR*

Porphyromonas gingivalis cells were grown to the mid-exponential phase. Total RNA was isolated from the harvested cells using an RNeasy Mini Kit (Qiagen Sciences, Valencia, CA, USA) and reverse-transcribed in a reaction mixture containing a random primer (Promega Co., Madison, WI, USA), dNTP mixture, RNase inhibitor (Wako Pure Chemical Industries, Ltd., Osaka, Japan), dithiothreitol, Superscript II (Invitrogen, Carlsbad, CA, USA), and DEPC-treated water. Real-time quantitative PCR was performed using Full Velocity SYBR Green QPCR Master Mix (Stratagene, La Jolla, CA, USA) according to the manufacturer's instructions. Primer sequences for the real-time PCR are listed in Supplementary Table S1. PCR amplification was performed in the following setting: preheating (95°C for 5 min) and 30 cycles of DNA denaturation (95°C for 10 s), and primer annealing/DNA extension (60°C for 30 s). The expression level of each targeted gene was normalized to that of the 16S rRNA gene. The comparative cycle threshold method[37] was used for relative quantification.

2.5. *Nucleotide sequence accession numbers*

The fully annotated genome sequence of *P. gingivalis* strain ATCC 33277 has been deposited in GenBank/EMBL/DDBJ databases under the accession number AP009380. Nucleotide sequences of the glucose kinase-encoding genes (*glk*) of five *P. gingivalis* strains have been deposited under the accession numbers AB293447 (strain TDC60), AB293448 (TDC117), AB293449 (TDC275), AB293450 (SU63), and AB293451 (GAI7802).

3. Results and discussion

3.1. *General features of the ATCC 33277 genome*

The genome of ATCC 33277 comprised a single circular chromosome of 2 354 886 bp with an average G + C content of 48.4% (Fig. 1). The size was almost the same as that of W83 (2 343 476 bp). The ATCC 33277 genome contained 2090 CDSs (PGN No.) with an average size of 970 bp, covering 86.1% of the whole chromosome sequence. It contained 4 RNA operons (*rrn*, 5S rRNA-23S rRNA-tRNA^{Ala}-tRNA^{Ile}-16S rRNA) and 53 tRNA genes that provide specificity for all kinds of amino acids. The numbers of *rrn* operons and tRNA genes were identical to those of W83. By the χ^2 analysis, we identified 13 regions with atypical nucleotide composition on the ATCC 33277 chromosome (Fig. 1, 8th circle). Many genes in the regions exhibited higher similarity to the genes in other bacterial species such as *B. fragilis* than those in strain W83, suggesting that they have been introduced to ATCC 33277 by horizontal gene transfer.

3.2. *Strain-specific CDSs*

To more precisely compare the CDS sets encoded on the ATCC 33277 and W83 genomes, we reannotated CDSs on the W83 genome by the same criteria as those used for ATCC 33277. We detected 114 CDSs (PGa No.) in the W83 genome that had not been annotated by Nelson et al.[19] They included many fragments of transposases of insertion sequences (ISs) but at least 27 function-assignable genes, such as those for translocase SecE subunit, pseudouridine

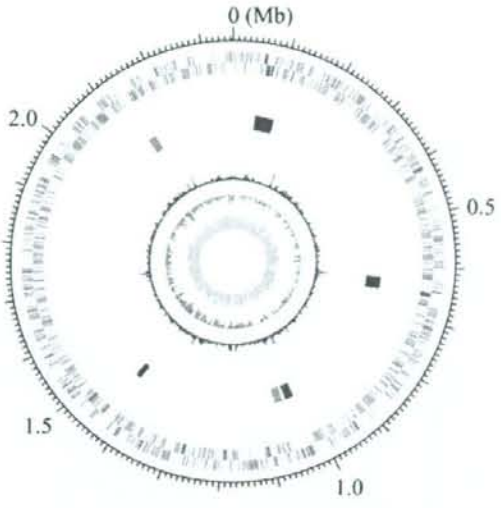

Figure 1. Circular map of the chromosome of *P. gingivalis* strain ATCC 33277. From the outside, the first and second circles show CDSs on the plus and minus strands, respectively. CDSs conserved in strains ATCC 33277 and W83 are indicated in red and ATCC 33277-specific CDSs in blue. The 3rd to 5th circles show IS elements (orange, IS*Pg1*; light green, IS*Pg2*; magenta, IS*Pg3*; cyan, IS*Pg4*; brown, IS*Pg5*; blue, IS*Pg6*), MITEs (magenta, MITE239; black, MITE*PgRS*; cyan, MITE700), CTns, and Tns (blue, CTnPg1-a, CTnPg1-b, CTnPg2, and CTnPg3; red, Tn*Pg17*), respectively. The 6th and 7th circles show *rrn* operons and tRNA genes, respectively. The 8th circle shows the result of χ^2 analysis of nucleotide composition. Regions exhibiting values of >600 are indicated in red and those of <600 are indicated in blue. The G + C skew and G + C content are shown in the 9th and 10th circles, respectively.

synthases, and lysine-specific cysteine proteinase (Supplementary Table S2). In total, we identified 2023 CDSs in W83.

ATCC 33277 and W83 genomes had a number of multi-copied CDSs such as those for IS transposases. ATCC 33277 and W83 contained 53 and 32 multi-copied CDS groups, respectively; the gene products of each group exhibited ≥ 90% amino-acid sequence identity (Supplementary Tables S3 and S4). In bidirectional best-hit analysis to identify conserved CDSs between the two strains, we used the largest CDS in each multi-copied CDS group as the representative of each group. By the analysis, we identified 1490 conserved CDSs, 461 ATCC 33277-specific CDSs, and 415 W83-specific CDSs. The strain-specific CDSs are listed in Supplementary Tables S5 and S6, respectively.

Most of the strain-specific CDSs encoded hypothetical proteins of unknown functions, but function-predictable W83-specific CDSs included several genes that may be related to the higher virulence of the strain, such as those for glycosyltransferase (PG0110), a protein required for capsular polysaccharide biosynthesis (PG0111), sensor histidine kinase (PG0719), surface antigen PgaA (PG0742), and thiol protease (PG1055). The two strains encoded different sets of DNA restriction-modification system proteins.

3.3. *CTn and transposon*

ATCC 33277 contained a variety of mobile genetic elements. We found four copies of CTns that were absent in W83 (Fig. 2). CTnPg1-a is 44.3 kb in size and encodes 50 CDSs (PGN_0046 to PGN_0095), including a set of genes for conjugative transfer and integration as well as those for an Na^+-driven multi-drug efflux pump. Several genes showed moderate sequence homologies to the genes of CTns of *Bacteroides* species.[38–40] CTnPg1-b, which is 9.7 kb in size and encodes 15 CDSs (PGN_1281 to PGN_1295), is identical to a part of CTnPg1-a (PGN_0046 to PGN_0060). One end of CTnPg1-b has been disrupted by multiple IS insertions. We identified two additional CTns, CTnPg2 and CTnPg3, but both were also truncated and highly degraded by multiple IS insertions.

We identified two identical copies of a novel composite transposon (Tn) named Tn*Pg17*-a and Tn*Pg17*-b in the ATCC 33277 genome. Tn*Pg17* is 16.8 kb in size and has IS*Pg3* at both ends. Target site duplications of 4 and 7 bp were found for Tn*Pg17*-a and Tn*Pg17*-b, respectively. Tn*Pg17* carries genes for a *tetR* family transcriptional regulator, ABC transporter ATP-binding proteins, and a carboxyl-terminal processing protease.

3.4. *IS and miniature inverted-repeat transposable element*

A total of 93 IS elements (including 38 partial copies) and 48 miniature inverted-repeat transposable elements (MITEs) (including 18 partial copies) were found in ATCC 33277 (Table 1). The IS elements identified were classified into six types, IS*Pg1*–IS*Pg6*, all of which are also present in W83.[19] MITEs comprise a group of small mobile genetic elements and are massively amplified often in plants.[41] They do not encode transposases by themselves but have terminal inverted repeats (TIRs) that are the same as or very similar to those of some IS elements, and they are thus transposable by the action of transposase provided *in trans* by the cognate IS element. In ATCC 33277, we identified three types of MITEs, MITE239, MITE700, and MITE464, all of which have also been identified on the W83 genome.[19] The structure of MITE239 was well conserved between the copies, 239 bp in length and with the same TIR as